# Reflectance anisotropy spectroscopy of Si(111)-(3 × 1)Li and Ag surfaces

S. Jorgji, J. F. McGilp, and C. H. Patterson
*School of Physics, Trinity College, Dublin 2, Ireland*
(Received 26 January 2013; revised manuscript received 20 March 2013; published 8 May 2013)

The Si(111)-(3 × 1)Li and Ag surface structures consist of Si honeycomb chains separated by channels occupied by Li or Ag atoms. The dimerization of neighboring Ag atoms results in a larger $c(12 \times 2)$Ag superstructure. We report calculations of the electronic surface states, dielectric function, and reflectance anisotropy spectrum of these surfaces using hybrid density functional theory (DFT) methods. The positions of surface states and the reflectance anisotropy spectrum calculated using DFT are in very good agreement with experimental results, where they have been reported. The surface states which contribute to the reflectance anisotropy below the band gap are identified for each orientation of the incident electromagnetic field.

DOI: 10.1103/PhysRevB.87.195304 PACS number(s): 78.68.+m, 73.20.At

## I. INTRODUCTION

The Si(111)-(3 × 1)Li and Ag surface reconstructions have been known for over 20 years.[1–3] Their structure consists of Si atoms in honeycomb chains separated by Li or Ag atoms in intervening channels.[4,5] Honeycomb chains in the honeycomb chain channel (HCC) structure consist of planar, six-membered rings, which lie parallel to the surface and are separated by channels which contain metal atoms (Figs. 1 and 2). Electronic surface states for this reconstruction have been calculated using density functional theory (DFT)[6–8] and observed by angle resolved photoelectron spectroscopy (ARPES).[9–11] Comparison of ARPES data for the Si(111)-(3 × 1)M surfaces, where M = Ag (Ref. 10), Li (Ref. 11), or Na (Ref. 9), shows that they have very similar electronic surface states.

There is evidence that the (3 × 1) reconstruction is not the ground state of the Ag covered Si(111) surface at 1/3 of a monolayer from low energy electron diffraction (LEED), scanning tunneling microscopy (STM), and DFT calculations.[8,12–15] A (3 × 1) to (6 × 1) phase transition is observed around 500 K and a (6 × 1) to $c(12 \times 2)$ phase transition around 100 K (Ref. 13). DFT calculations by Chuang and coworkers[8] found total energies for (6 × 1) and $c(12 \times 2)$ HCC structures which are 190 and 219 meV per (6 × 2) cell lower in energy than the (3 × 1) HCC structure. The driving force for further surface reconstruction is the displacement of Ag atoms along channels to form dimers.[4] The ordering of displacements results in large supercells.

Here we report calculations of the electronic surface states, surface dielectric function and reflectance anisotropy (RA) spectrum of the Si(111)-(3 × 1)Li and Ag surfaces. The computed RA spectrum for the (3 × 1)Ag surface is in good agreement with previously reported experimental RA data for this surface;[16,17] the RA spectrum for the (3 × 1)Li surface has not been reported in the literature, however, strong similarities in the surface electronic structures of the Ag and Li systems and their surface dielectric functions result in similar predicted RA spectra. The origins of the features of the RA spectra below the bulk band gap are identified in terms of transitions between surface states associated with the HCC and chains of Li or Ag atoms. The RA spectrum was also calculated for the $c(12 \times 2)$Ag reconstruction, which reveals the extent to which the RA spectrum depends on Ag positions in channels.

RA spectroscopy[18] is a linear optical technique which can be used to probe optical excitations at crystal surfaces[19] when the response of the underlying bulk to normal incidence electromagnetic fields is independent of polarization direction. This is the case in cubic crystal systems. For example, the difference in reflectivity is measured for light polarized parallel or perpendicular to a mirror plane of symmetry perpendicular to the surface. RA spectra can be interpreted in terms of transitions between electronic surface states when the anisotropic surface dielectric function and band structure are available.

The surface reflectivity anisotropy $\frac{\Delta r}{r}$ is[19]

$$\frac{\Delta r}{r} = 2\frac{r_x - r_y}{r_x + r_y}, \tag{1}$$

where $r_\alpha$ ($\alpha = x, y$) is the complex reflection coefficient along a particular axis. The normalized change in reflectance, $\frac{\Delta R}{R}$, induced by a thin surface layer with the electric vector aligned along Cartesian $x$ or $y$ axes is,

$$\frac{\Delta R_{x,y}}{R} = 2\mathrm{Re}\frac{\Delta r}{r} = 4kd\,\mathrm{Im}\frac{\left(\Delta\chi^i_{xs}\chi^r_b - \Delta\chi^r_{xs}\chi^i_b\right)}{|\chi_b|^2}, \tag{2}$$

where the superscripts $r$ and $i$ indicate real and imaginary parts, $k$ is the wave-vector magnitude of the incident light, and $d$ is the surface layer thickness. The frequency-dependent surface excess susceptibility[20] is defined by

$$\chi_{xs,\alpha}(\omega) = \chi_{s,\alpha}(\omega) - \chi_b(\omega). \tag{3}$$

The surface excess susceptibility difference for the two electric field orientations reduces to the difference in slab susceptibilities

$$\Delta\chi_{xs}(\omega) = \chi_{s,x}(\omega) - \chi_{s,y}(\omega). \tag{4}$$

The susceptibility of bulk, $\chi_b$, or slab, $\chi_s$, structures used in calculations is

$$\chi_\alpha(\omega) = \frac{2e^2}{m^2\epsilon_o\Omega\omega^2}\sum_{nn'\mathbf{k}}\frac{[f_o(E_{n\mathbf{k}}) - f_o(E_{n'\mathbf{k}})]\left|p^\alpha_{nn'\mathbf{k}}\right|^2}{(E_{nn'\mathbf{k}} - E - i\delta)}, \tag{5}$$

where $f_o$ is a Fermi occupation factor, $p^\alpha_{nn'\mathbf{k}}$ is a momentum matrix element connecting states $n\mathbf{k}$ and $n'\mathbf{k}$ in the presence of a field along direction $\alpha$, $E_{nn'\mathbf{k}}$ is the corresponding transition energy, and $m$, $e$ and $\Omega$ are the electron mass, charge, and unit cell volume.

 

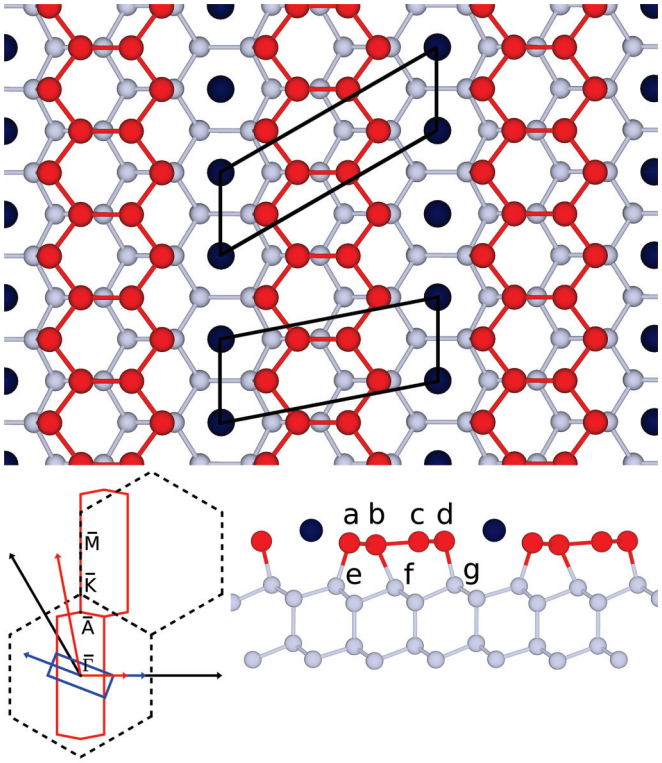


FIG. 1. (Color online) (Top panel) Surface structure of Si(111)-(3 × 1)Li with a (3 × 1) net and the primitive unit cell outlined. (Bottom left panel) Reciprocal lattice vectors and surface Brillouin zones for (1 × 1) (black dotted lines), (3 × 1) (red solid lines), and $c(12 \times 2)$ (blue rectangle) surface unit cells. (Bottom right panel) Side view of the Si(111)-(3 × 1)Li surface. Li atoms (dark blue), Si HCC atoms (red), first Si bilayer atoms (light grey).

## II. COMPUTATIONAL DETAILS

The slabs used for surface electronic structure calculations contained 6, 9, or 12 bulk Si bilayers plus terminating HCC or modified H atom layers. The H atom basis set and Si-H distance were modified so that Mulliken populations of Si atoms at the H-terminated surface were as close as possible to the bulk value. All atom positions in the slab unit cells, with

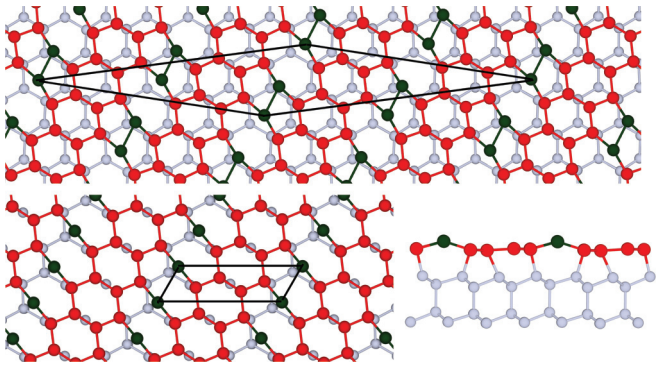

FIG. 2. (Color online) Structures of $c(12 \times 2)$ and (3 × 1) surface unit cells obtained from geometry optimization calculations. (Top panel) $c(12 \times 2)$ unit cell with dimerized Ag atoms. (Bottom panel) (3 × 1) unit cell, plan, and side views. Ag (dark green), Si HCC layer (red), Si bulk layer (light grey).

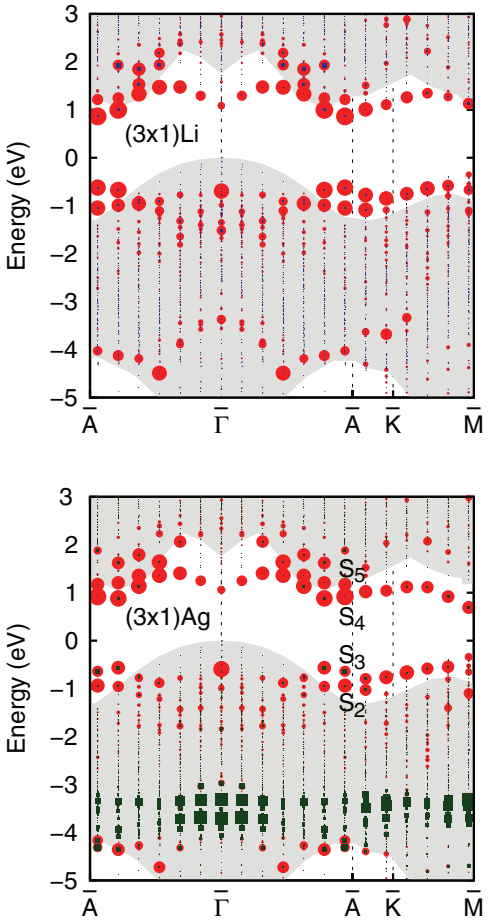


FIG. 3. (Color online) (Top panel) Si(111)-(3 × 1)Li band structure for $k$ vectors parallel to Li chains and $[\bar{1}10]$ direction. (Bottom panel) Si(111)-(3 × 1)Ag band structure parallel to Ag chains. The degree of wave-function localization on HCC atoms and Li or Ag atoms is indicated by circle and square size, respectively. Sizes of Ag squares are scaled by one half relative to Si HCC. States labeled $S_2$ to $S_5$ are described in the text.

the exception of terminating H atoms and their Si nearest neighbors, were allowed to relax in energy minimization calculations. The electronic band structures shown in Fig. 3 were obtained using a nine bilayer slab terminated with an H atom and HCC surface layers. A similar slab terminated with the (3 × 1) or $c(12 \times 2)$ structures on *both* surfaces was used for slab dielectric susceptibilty calculations. In those cases the surface states are split to a very small extent over most of the surface Brillouin zone (SBZ) because there are two equivalent surfaces. The structures in Figs. 1 and 2 were drawn using the VESTA software package.[21]

Surface and bulk dielectric susceptibilities were calculated using the EXCITON code[22] using a 16 × 36 grid of $k$ points in the surface Brillouin zone and a 24 × 24 × 24 grid in the bulk Brillouin zone. Integration over the Brillouin zone was performed using an interpolation method.[23] Extensive tests of the dependence of the RA spectrum on slab thickness, $k$-point sampling density, and surface termination by HCC and H or by HCC and HCC were performed in this work. RA spectra for 6, 9, and 12 Si bilayer thickness were very similar. In the following section we present a graphical representation

of the transition matrix elements over the SBZ. We found very good agreement between RA spectra obtained using slabs which were terminated by HCC and H or by HCC and HCC, especially in the sub-band-gap region.

All self-consistent field calculations were performed using the CRYSTAL program.[24] The basis set for Si is described in Ref. 25. The basis set for Ag is a modified version of the basis for the Hay-Wadt small core pseudopotential[26] for Ag. It is unpublished but is available on the CRYSTAL website.[24] The basis for Li is described in Ref. 27.

The Becke-3 Lee, Yang, and Parr (B3LYP) hybrid density functional[28,29] contains a Hartree-Fock exchange with weight $A$, the local density approximation to exchange[30] $E_x^{\mathrm{LDA}}$, with weight $(1-A)$; Becke's gradient corrected exchange functional[31] $E_x^{\mathrm{Becke}}$, with weight $B$; the Lee, Yang, and Parr approximation to the correlation functional[32] $E_c^{\mathrm{LYP}}$, with weight $C$; and the Vosko, Wilks, and Nusair approximation to the electron correlation functional[33] $E_c^{\mathrm{VWN}}$, with weight $(1-C)$,

$$E_{xc} = (1-A)\left(E_x^{\mathrm{LDA}} + B E_x^{\mathrm{Becke}}\right) + A E_x^{\mathrm{HF}} + (1-C) E_c^{\mathrm{VWN}} + C E_c^{\mathrm{LYP}}. \quad (6)$$

The B3LYP functional contains a Fock exchange with a weight $A = 0.2$; this results in an overestimation of the indirect band gap of bulk Si by 0.7 eV. This was reduced to $A = 0.05$, which results in good agreement with the experimental indirect band gap and dielectric function of bulk Si. The B3LYP hybrid density functional, with $A = 0.05$, and $B$ and $C$ fixed at their standard values, is used throughout this work, and has been used successfully for other Si surface structures.[34] The indirect band gap is 1.14 eV and is in good agreement with the experimental value of 1.17 eV (Ref. 35), while the direct gap at the $\Gamma$ point, 2.90 eV, is underestimated compared to the experimental value of 3.4 eV. The static, long wavelength dielectric function is 11.8, compared to the experimental value of 11.4 and the $E2$ peak position, 4.38 eV, is in reasonable agreement with the experimental value 4.25 eV. The intensity of the $E1$ peak is underestimated, compared to the experiment. However, all single-particle calculations of the dielectric function of bulk Si omit the electron-hole attraction effects which are necessary to reproduce this feature of the $\epsilon_2$ spectrum.

## III. RESULTS

### A. Atomic structure

Structures of the $(3 \times 1)$Li and Ag and $c(12 \times 2)$Ag phases obtained by total energy minimization are shown in Figs. 1 and 2. The spacing of Li or Ag atoms along the channels in the $(3 \times 1)$ phase is 3.83 Å, the Si–Si next nearest neighbor spacing. The preferred site for Li atoms is a nearly three-fold symmetric site shown in Fig. 1 where the Li atom is 2.78 Å from one Si HCC atom and 2.91 Å from two Si HCC atoms. An alternative site where the Li is shifted by half a lattice spacing along the channels was not studied. Lottermoser *et al.* reported DFT calculations for this Li site, although they were unable to determine the Li registry from soft x-ray diffraction measurements or low energy electron diffraction owing to its low scattering strength. We find that the potential energy surface for Li in the channel is very flat as the interaction between Li and the rest of the surface is ionic rather than covalent.

The preferred site for Ag atoms is the low symmetry site where the Ag atom is located midway between two Si HCC atoms, as shown in Fig. 2. Ag atoms placed in a nearly three-fold site favored by Li resulted in displacement into the low symmetry site.

Si HCC atoms form very similar structures for both adsorbates and have similar bond lengths to the topmost Si bilayer. Si–Si bond lengths in HCC rings range from 2.36 to 2.44 Å, with a mean value of 2.39 Å in Si(111)-$(3 \times 1)$Ag and from 2.34 to 2.40 Å, with a mean value of 2.37 Å in Si(111)-$(3 \times 1)$Li. These distances are similar to the relaxed bulk Si–Si bond length in the slab 2.38 Å, which is an overestimate compared to the bulk Si–Si bond distance of 2.35 Å. Th overestimation of the experimental bond lengths by 1 to 1.5% is typical of the hybrid DFT method used here, while DFT tends to underestimate bond lengths.

The bond distances that we find for Si(111)-$(3 \times 1)$Li are mostly very similar to the bond lengths derived from the coordinates in Table I of Ref. 5. The bond lengths found in this work are 0.01 to 0.02 Å longer than those in Ref. 5, as can be expected from DFT versus hybrid DFT calculations, except for the distance between the atom in the honeycomb which is shown without a bond to the Si top bilayer in Fig. 1 (the bond between Si3 and Si6 in the 560560 structure in Ref. 5 or atoms $c$ and $f$ of this work). We find a long distance of 2.82 Å compared to 2.58 Å. Other bond lengths between the honeycomb atoms and the top bilayer are in agreement.

The dimerized $c(12 \times 2)$Ag structure was obtained when atoms with the relaxed $(3 \times 1)$ cell positions were allowed to relax further in a $c(12 \times 2)$ cell. The Ag–Ag distance in the dimers is 3.04 Å, which is 5% larger than the Ag–Ag distance in bulk Ag (2.88 Å). The energy lowering on relaxation from the undimerized to dimerized geometry was 110 meV per dimer. Si–Ag bond lengths in the $(3 \times 1)$ unit cell are 2.61 and 2.62 Å. Si–Ag bond lengths in the $c(12 \times 2)$ unit cell are around 2.60 and 2.68 Å with the latter bond length increasing to accommodate the Ag dimer formation. Si–Si bond lengths in HCC rings in the $c(12 \times 2)$ phase are similar to those in the $(3 \times 1)$ phase.

### B. Electronic structure

The electronic band structures of a Si(111) slab terminated by the $(3 \times 1)$-Li and Ag structures for wave vectors parallel to Li or Ag chains are shown in Fig. 3. The red circles in Fig. 3 indicate the extent of localization of the wave function on HCC atoms and dark green or dark blue squares indicate the extent of localization on Li or Ag atoms. Projected bulk band energies, obtained using the same hybrid DFT Hamiltonian and basis set, are shown as shaded regions. The similarities in the HCC band structures are striking. Over most of the range of $k$ space shown, there are two occupied and two vacant surface states just above or below the valence and conduction band edges. These states become surface resonances around the $\overline{\Gamma}$ point of the SBZ. There is a surface state in both systems around the edge of the bulk projected bands about 4 eV below the Fermi level. In the $(3 \times 1)$Ag system, this state crosses

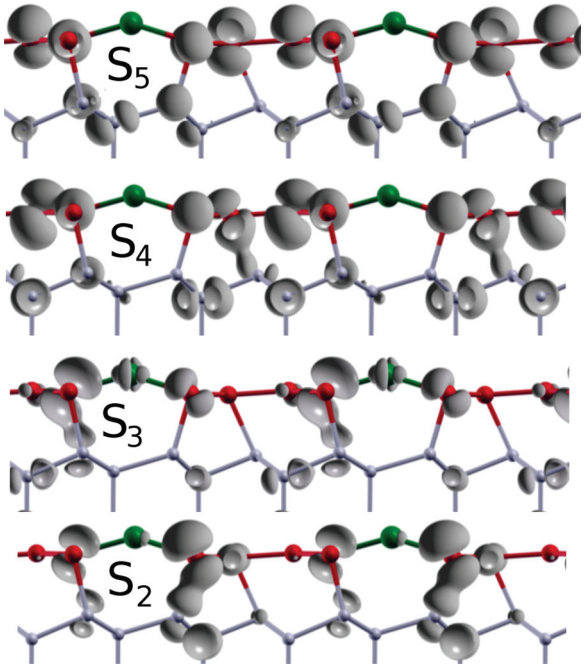


FIG. 4. (Color online) Isosurface plots of modulus squared of surface states for Si(111)-(3 × 1)Ag close to the $\overline{\mathbf{A}}$ point of the SBZ. States labeled $S_2$ to $S_5$ are described in detail in the text. Ag atoms (green), HCC Si atoms (red), first bilayer Si atoms (light grey).

nondispersing Ag 4*d* bands and hybridizes with them forming surface resonance states just above and below the Ag 4*d* bands. The surface states and resonances at the band edges are mainly localized on HCC atoms; only the highest occupied state close to the $\overline{\mathbf{A}}$ point of the (3 × 1)Ag system has any significant weight on Ag atoms. There is very little localization of any valence or conduction band state on Li ions in the energy range shown for the (3 × 1)Li system, indicating that Li exists essentially as $Li^+$.

Plots of the modulus squared of two pairs of surface states in the (3 × 1)Ag system, above and below the Fermi level close to the $\overline{\mathbf{A}}$ point, are shown in Fig. 4. These states are labeled $S_2$ to $S_5$ to match the notation used previously in Ref. 7. $S_1$ is a surface resonance (not shown), which is similar to states labeled $S_1^+$ and $S_1$ in Refs. 6 and 7. It has a small degree of surface localization compared to the true surface states in the bulk band gap. States $S_2$ and $S_3$, which are occupied, are mainly localized on HCC Si atoms bonded to Ag atoms. State $S_2$ is approximately odd with respect to reflection in a mirror plane perpendicular to the surface which passes through a chain of Ag atoms along the $[\bar{1}10]$ direction. It has very little Ag 4*d* character. State $S_3$ is approximately even with respect to this mirror plane and has an Ag $4d_{z^2}$ character, if the Si–Ag–Si bonds lie along a local *z* direction. Similar plots for the (3 × 1)Li system, which are not shown here, reveal a similar character for its surface states. We also find a surface resonance state below states $S_2$ and $S_3$, which is similar to the states labeled $S_1^+$ and $S_1$ in Refs. 6 and 7, although this state has a small degree of surface localization compared to the true surface states in the bulk band gap.

A pair of surface states has been observed in ARPES of the Si(111)-(3 × 1)Ag surface just above the projected bulk states and at 4 eV below the Fermi level. These states were labeled $SS_1'$, $SS_2'$, and $SS_3'$ (Ref. 10). ARPES studies of Si(111)-(3 × 1)*M* surfaces, where *M* = Li or Na, show either one[11,36] or three[9] surface states in this region of the SBZ. DFT calculations on Si(111)-(3 × 1)Li (Ref. 6) and Na (Ref. 7) surfaces show three filled and one vacant surface states in this region of the SBZ. Erwin and Weitering[6] have argued that two of the three states found in DFT should be observed in ARPES owing to their parity with respect to an approximate mirror plane of symmetry perpendicular to six membered rings in HCC. DFT calculations on Si(111)-(3 × 1)Ag (Ref. 8) find two filled and two vacant surface states. Orbital plots for the alkali metal systems[6,7] show that surface state orbitals on HCC atoms are very similar to those for the Ag system shown in Fig. 4.

### C. Dielectric function and reflectance anisotropy

The imaginary parts of dielectric functions for slabs with both surfaces terminated by the (3 × 1)Li or Ag phases is shown in Fig. 5 for the electric vector aligned either parallel to (along $[\bar{1}10]$) or perpendicular to (along $[11\bar{2}]$) Li or Ag chains (Figs. 1 and 2). Sub-band-gap peaks corresponding to transitions between surface states are observed at 1.5 eV, for the electric vector parallel to Ag chains, and at 1.8 eV, for the electric vector perpendicular to Ag chains. A similar

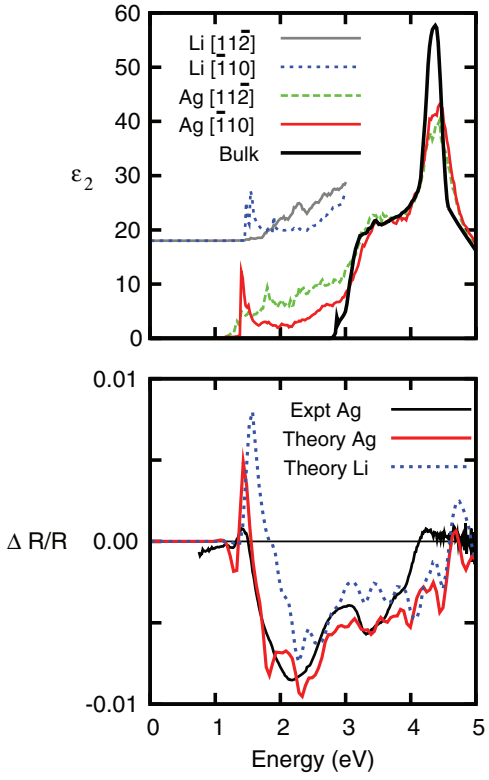


FIG. 5. (Color online) Imaginary part of the dielectric function and RA spectra for Si(111)-(3 × 1)Li and Ag with the electric vector of incident radiation parallel to $[\bar{1}10]$ and $[11\bar{2}]$ crystallographic directions. (Top panel) Dielectric functions from slab calculations for both systems. (3 × 1)Li data have been offset. (Bottom panel) RA spectra from experiment (Ref. 16) and calculations using Eq. (2).

sub-band-gap transition is observed at 1.6 eV for the electric vector parallel to Li chains, however, there is no peak for the electric vector perpendicular to Li chains, corresponding to the peak at 1.8 eV in the Ag system. Furthermore, the onset for sub-band-gap optical absorption occurs at a higher energy than in the Ag system.

RA spectra for the Si(111)-(3 × 1)Ag surface from experiment[16] and for both (3 × 1)Ag and (3 × 1)Li systems calculated using these dielectric functions are also shown in Fig. 5. In general, there is more structure in the theoretical spectra than is found experimentally. The theoretical RA spectrum shows similar negative and positive peaks to those in the experimental curve around 1.5 eV, although the amplitudes of the experimental peaks are significantly smaller. While the (3 × 1)Ag and (3 × 1)Li systems have quite similar surface state electronic structures, there are differences in their sub-band-gap dielectric functions (Fig. 5). The sensitivity of the dielectric function to surface state character, the degree of surface order or thermal effects may explain the difference in theory and experiment for the (3 × 1)Ag system. RA spectra in this energy range are easily interpreted in terms of peaks in the imaginary part of the surface dielectric functions as the bulk dielectric function is entirely real at this energy. In this case the RA signal is proportional to the difference in imaginary parts of the dielectric function [Eq. (2)]. Thus the small negative dip at 1.3 eV in the (3 × 1)Ag system occurs because the onset of optical transitions for the electric vector aligned perpendicular to the Ag chains occurs just before that for the other electric vector alignment. For the (3 × 1)Li system, however, there is no negative dip at the onset of the optical anisotropy because optical transitions for the electric field perpendicular to Li chains begin at a higher energy.

The positive peak at 1.5 eV in the (3 × 1)Ag system is caused by the onset of transitions at 1.5 eV with the electric vector aligned parallel to Ag chains. The theoretical RA spectrum has a negative peak at 1.8 eV where the experimental spectrum has a strong dip. There is a second negative peak in the experimental RA spectrum at 3.5 eV, which is also found in the theoretical spectrum where it is due to the difference in the surface dielectric function around the $E1$ peak of the bulk dielectric function. The experimental data were obtained from a vicinal substrate, which was used to form a single domain, and it is known that transitions associated with step structure occur in this spectral region.[37] However, the offcut in this case was only 1° and the spectra show no significant step contribution.[16,17]

A plot of the modulus squared of the transition matrix element in Eq. (5), $p^{\alpha}_{nn'\mathbf{k}}$, between the occupied and vacant states with transition energies of 1.50 ± 0.05 eV with the electric vector of the radiation aligned parallel or perpendicular to Ag chains, is shown in Fig. 6. The plots show that the strongest transitions are localized around the $\overline{\mathbf{A}}$ point of the SBZ when the electric vector is parallel to the $[\bar{1}10]$ direction, with a weaker contribution around the $\overline{\mathbf{M}}$ point. When the electric vector is aligned perpendicular to the chains, along the $[11\bar{2}]$ direction, the transition matrix elements are largest around the $\overline{\mathbf{M}}$ point of the SBZ.

The energy gap between the occupied surface state $S_3$ and the empty surface state $S_4$ around the $\overline{\mathbf{A}}$ point is 1.5 eV. The analysis of contributions to the peak in the $\epsilon_2$ spectrum with

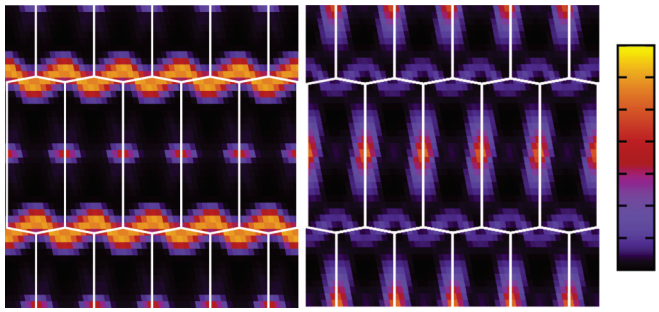

FIG. 6. (Color online) Modulus squared of the transition matrix element $p^{\alpha}_{nn'\mathbf{k}}$ between occupied and vacant surface states in Si(111)-(3 × 1)Ag over several unit cells in reciprocal space for optical transitions at 1.50 ± 0.05 eV. (3 × 1) SBZ are shown as white lines. (Left panel) Field parallel to Ag chains and $[\bar{1}10]$, (right panel) field parallel to $[11\bar{2}]$.

the electric vector parallel to the $[\bar{1}10]$ direction at that energy shows that this peak is entirely caused by transitions between these surface states. The energy gap between occupied and vacant surface states around the $\overline{\mathbf{M}}$ point of the SBZ is larger (1.8 eV) and there are contributions from transitions between states which resemble both the occupied $S_2$ and $S_3$ and the empty $S_4$ state in Fig. 3 at this energy and this region of the SBZ. The vacant "$\pi^*$" state $S_5$ does not contribute to either of the peaks in the $\epsilon_2$ spectrum.

To determine the extent to which the ordering of displacements of Ag atoms along HCC channels affects the optical response of the system, the RA spectrum was calculated using $c(12 \times 2)$ unit cells for both the dimerized and undimerized Ag chains shown in Fig. 2. The undimerized chain system had exactly the same structure as the relaxed (3 × 1) system. Only a minor difference in the RA spectra in the sub-band-gap energy range was found between dimerized and undimerized $c(12 \times 2)$ unit cells. This is likely to be because the surface states which cause the optical anisotropy in the surface at this energy are predominantly of Si $3p$ character on HCC atoms.

While the room temperature surface is predominantly (3 × 1), significant areas of (6 × 1) and $c(12 \times 2)$ periodicity are also generally found experimentally. Good agreement between the theory and experiment for the sub-band-gap region is understandable if these transitions arise from the HCC atoms, which have essentially the same structure for all three reconstructions.

## IV. DISCUSSION AND CONCLUSION

In this section we discuss the electronic structure of HCC systems, compare the results of our surface state calculations to ARPES data and previous DFT calculations on HCC systems, and note which surface states contribute to optical anisotropy in HCC systems.

Figures 1 and 4 show Si–Si bonds connecting HCC atoms to the top bulk Si bilayer. They form alternating five- and six-membered rings perpendicular to the surface. Bond lengths between HCC and top bilayer atoms, using the atom labels in Fig. 1, are as follows: $a$-$e$ 2.45, $b$-$f$ 2.58, $c$-$f$ 2.82, and $d$-$g$ 2.43 Å in the (3 × 1)Ag system. Very similar values are found in the (3 × 1)Li system. One pair of Si atoms in each HCC

ring ($c$-$f$) is a much larger distance (2.82 Å) from the nearest top Si bilayer atom and is not covalently connected to the layer beneath.

States $S_4$ and $S_5$ are vacant and are localized on HCC atoms. State $S_4$ is localized mainly on HCC atoms which lack covalent bonding to the layer beneath as well as the long (2.58 Å) bilayer-HCC atom bond. State $S_5$ is a "$\pi^*$" state of the HCC ring. The label $\pi$ is used tentatively here as these electrons in the Si $3p$ states perpendicular to the HCC rings are all used in bonding HCC rings to Si bilayer atoms.

Ag atoms are monovalent and are bonded to HCC Si atoms via pairs of dative-covalent bonds; Li atoms are also monovalent, but have an ionic interaction with the HCC atoms. HCC atoms at channel edges in the $(3 \times 1)$Li system have electron lone pairs instead of dative-covalent bond pairs. The evidence for these pairs is provided by a Mulliken population analysis of these Si atoms: Si HCC atoms at channel edges in the $(3 \times 1)$Li system (atoms $a$ and $d$) have excess charges of 0.20 and 0.27 $e$, respectively, while atoms at channel edges in the $(3 \times 1)$Ag system have smaller excess charges (0.09 and 0.07 $e$). Excess charges on these atoms in the Ag system are smaller because this pair of electrons is part of a dative covalent bond to Ag atoms.

Electron counting shows that we expect one vacant "$\pi$" state per HCC ring. The four unique Si atoms in HCC rings contribute 16 valence electrons and each Li or Ag atom contributes one valence electron to bond formation. There are seven HCC $\sigma$ bonds per surface unit cell, including the two dative-covalent bonds to Ag or two HCC lone pairs in the Li system, which can be seen by inspecting one unit cell in the plan views of the structures in Figs. 1 and 2. This requires 14 valence electrons, leaving three electrons available for bonding to atoms in the bilayer below. As noted above, there are three Si bilayer to HCC ring bond lengths of 2.43 to 2.58 Å and one long nonbonded distance of 2.82 Å between one HCC ring atom and the closest bilayer atom. This atom is expected to be electron deficient as it has $\sigma$ bonds to three neighboring atoms and no bond to the bilayer below it. The evidence for electron deficiency in this atom is again provided by a Mulliken population analysis. The atoms labeled $c$ in Fig. 1 have electron deficits of 0.06 and 0.05 $e$ in the $(3 \times 1)$Li and Ag systems, respectively, while the other atoms labeled $b$ in the interior of the HCC rings have deficits of 0.02 $e$ for both systems. Since there is a formal deficit of one electron pair for the HCC ring atom without a bond to the Si bilayer below, we expect a low-lying vacant state with a character similar to that of state $S_4$ in Fig. 4. Lone pair surface states labeled $S_2^{\pm}$ (Ref. 6) [or $S_2$ and $S_3$ (Ref. 7)] in previous reports on alkali metal systems are equivalent to Si–Ag–Si bonding states $S_2$ and $S_3$. The vacant state labeled $S_1^-$ (Ref. 6) [or $S_4$ (Ref. 7)] is a "$\pi^*$" state in both Ag and alkali metal systems.

The orbital character of surface states $S_2$ and $S_3$ in Fig. 4 shows that they mainly comprise the lone pair on Si atoms at channel edges in the Li system and the dative covalent bond pair on similar atoms at channel edges in the Ag system. The lowest empty surface state $S_4$ is mainly localized on the electron deficient atoms in the HCC ring. The electron deficit from a Mulliken population analysis 0.06 $e$ is much smaller than a full electron pair. However, in a nonpolar material such as Si, large charge excesses are not energetically favorable. Instead, the charge transfer to formally electron deficient atoms occurs in deeper lying occupied states leaving a small net charge deficit. State $S_4$ is the unoccupied level mainly responsible for optical anisotropy at sub-band-gap energies.

As noted in Sec. III B, ARPES data for the $(3 \times 1)$Ag system[10] show two surface states close to the Fermi level between the $\overline{\mathbf{A}}$ and $\overline{\mathbf{K}}$ points of the SBZ. ARPES data for $(3 \times 1)$-alkali-metal systems show a single, weakly dispersing surface state in this region of $k$ space close to the Fermi energy,[11,36] or two or three surface states,[9] depending on the photon energy. Our calculations show a pair of nearly degenerate surface states which split by several tenths of an electron volt around the $\overline{\mathbf{A}}$ point of the SBZ. The observation of a single state in some cases may be because of near degeneracy or, as Erwin and Weitering have suggested,[6] a low ARPES cross section for one of the states.

Previous DFT calculations of surface states in $(3 \times 1)$-Li (Ref. 6) and Na (Ref. 7) systems have reported three occupied and one vacant surface states close to the Fermi level between the $\overline{\mathbf{A}}$ and $\overline{\mathbf{K}}$ points of the SBZ. However, no degree of localization on HCC atoms is shown in that work. Another DFT calculation of the band structure of the $(3 \times 1)$Ag system,[8] which does indicate the degree of surface localization, finds two surface states (labeled $S_1$ and $S_2$) with dispersions similar to that shown in this work for the $(3 \times 1)$Ag system. It also finds two additional states within the projected bulk band region, labeled $S_3$ and $S_4$, which have a much smaller degree of surface localization. The lack of a common criterion for the "surface state" may explain the difference in the number of states found in each case. Occupied states $S_2$ and $S_3$ and vacant state $S_4$ in Ref. 7 and occupied states $S_2^-$ and $S_2^+$ and vacant state $S_1^-$ in Ref. 6 closely resemble states $S_2$, $S_3$, and $S_4$ in Fig. 4 in this work.

The experimental RA spectrum for the $(3 \times 1)$Ag system shown in Fig. 5 has a small negative dip before a positive peak at 1.5 eV. As noted in Sec. III C, this structure arises because the onset for optical transitions with the electric field perpendicular to Ag chains occurs first, which causes the RA signal to be negative, while at 1.5 eV strong surface state transitions with the field parallel to chains causes the RA signal to swing positive.

The reason for the overestimate in strength of these features in the theoretical spectrum compared to the experimental spectrum is not clear. However, an inspection of the theoretical RA spectrum for the $(3 \times 1)$Li system shows that the shape of the spectrum in this energy range is sensitively dependent on the onset energies for optical transitions relative to the surface state transition peak. In that case there is no dip before the peak at 1.6 eV. Our calculations accurately reproduce the position of this feature in the RA spectrum. The hybrid DFT Hamiltonian used in this work was chosen so that the bulk dielectric function was well reproduced; apparently this choice also allows a fairly accurate determination of energetic positions of surface states in this system.

We have shown that the RA spectrum of the Si(111)-$(3 \times 1)$Ag system obtained from our hybrid DFT calculations is in good agreement with experiment.[16] We have also shown that one particular surface state, state $S_4$ in Figs. 3 and 4, is the key vacant state for sub-band-gap optical transitions in this system.

The other "$\pi^*$" vacant surface state is not important in sub-band-gap transitions. No RA measurements for the $(3 \times 1)$Li system have been performed, as far as the present authors are aware. Finally, RA spectra in the sub-band-gap region were found to be insensitive to the dimerization of Ag atoms along the $[\bar{1}10]$ direction. This is likely because the surface states which contribute most to the RA spectrum are predominantly localized on HCC Si atoms.

## ACKNOWLEDGMENTS

All calculations were performed on the Kelvin cluster maintained by the Trinity Centre for High Performance Computing. This cluster was funded through grants from the Irish Higher Education Authority, through its PRTLI program. The project was supported by the Higher Education Authority under the PRTLI V program and by Science Foundation Ireland under Grant No. 11/RFP/PHY/3047.

[1] W. C. Fan and A. Ignatiev, Phys. Rev. B **41**, 3592 (1990).
[2] K. J. Wan, X. F. Lin, and J. Nogami, Phys. Rev. B **47**, 13700 (1993).
[3] H. H. Weitering, N. J. DiNardo, R. Peréz-Sandoz, J. Chen, and E. J. Mele, Phys. Rev. B **49**, 16837 (1994).
[4] C. Collazo-Davila, D. Grozea, and L. D. Marks, Phys. Rev. Lett. **80**, 1678 (1998).
[5] L. Lottermoser, E. Landemark, D. M. Smilgies, M. Nielsen, R. Feidenhans'l, G. Falkenberg, R. L. Johnson, M. Gierer, A. P. Seitsonen, H. Kleine, H. Bludau, H. Over, S. K. Kim, and F. Jona, Phys. Rev. Lett. **80**, 3980 (1998).
[6] S. C. Erwin and H. H. Weitering, Phys. Rev. Lett. **81**, 2296 (1998).
[7] M. H. Kang, J. H. Kang, and S. Jeong, Phys. Rev. B **58**, R13359 (1998).
[8] F. C. Chuang, C. H. Hsu, C. Z. Wang, and K. M. Ho, Phys. Rev. B **78**, 245418 (2008).
[9] T. Okuda, K. Sakamoto, H. Nishimoto, H. Daimon, S. Suga, T. Kinoshita, and A. Kakizaki, Phys. Rev. B **55**, 6762 (1997).
[10] M. Gurnett, J. B. Gustafsson, K. O. Magnusson, S. M. Widstrand, and L. S. O. Johansson, Phys. Rev. B **66**, 161101 (2002).
[11] C. Bromberger, J. N. Crain, K. N. Altmann, J. J. Paggel, F. J. Himpsel, and D. Fick, Phys. Rev. B **68**, 075320 (2003).
[12] K. Sakamoto, H. Ashima, H. M. Zhang, and R. I. G. Uhrberg, Phys. Rev. B **65**, 045305 (2001).
[13] N. Miyata, I. Matsuda, M. D'Angelo, H. Moorikawa, T. Hirahara, and S. Hasegawa, e-J. Surf. Sci. Nanotech. **3**, 151 (2005).
[14] A. Urbieta, K. Schulte, B. Grandidier, D. Deresmes, S. Erwin, and D. Stiévenard, Surf. Sci. **603**, 311 (2009).
[15] A. Urbieta, K. Schulte, B. Grandidier, D. Deresmes, S. Erwin, and D. Stiévenard, Surf. Sci. **603**, 1079 (2009).
[16] S. Chandola, J. Jacob, K. Fleischer, P. Vogt, W. Richter, and J. F. McGilp, Phys. Status Solidi B **242**, 3017 (2005).
[17] S. Chandola, J. Jacob, K. Fleischer, P. Vogt, W. Richter, and J. F. McGilp, J. Phys. Condens. Matter **18**, 6979 (2006).
[18] J. D. E. McIntyre and D. E. Aspnes, Surf. Sci. **24**, 417 (1971).
[19] P. Weightman, D. Martin, R. Cole, and T. Farrell, Rep. Prog. Phys. **68**, 1251 (2005).
[20] M. K. Kelly, S. Zoller, and M. Cardona, Surf. Sci. **285**, 282 (1993).
[21] K. Momma and F. Izumi, J. Appl. Crystallogr. **41**, 653 (2008).
[22] C. H. Patterson, Mol. Phy. **108**, 3181 (2010).
[23] J. Rath and A. J. Freeman, Phys. Rev. B **11**, 2109 (1975).
[24] R. Dovesi, V. R. Saunders, C. Roetti, R. Orlando, C. M. Zicovich-Wilson, F. Pascale, B. Civalleri, K. Doll, N. M. Harrison, I. Bush, P. D'Arco, and M. Llunell (2009), Crystal09 User's Manual, University of Torino, Torino (2009) www.crystal.unito.it.
[25] F. Pascale, M. Catti, A. Damin, R. Orlando, V. Saunders, and R. Dovesi, J. Phys. Chem. B **109**, 18522 (2005).
[26] P. J. Hay and W. R. Wadt, J. Chem. Phys. **82**, 299 (1985).
[27] M. F. Peintinger, D. V. Oliveira, and T. Bredow, J. Comput. Chem. **34**, 1 (2013).
[28] A. D. Becke, J. Chem. Phys. **98**, 5648 (1993).
[29] P. J. Stephens, F. J. Devlin, C. F. Chabalowski, and M. J. Frisch, J. Phys. Chem. **98**, 11623 (1994).
[30] P. A. M. Dirac, Proc. Cambridge Philos. Soc. **26**, 376 (1930).
[31] A. D. Becke, Phys. Rev. A **38**, 3098 (1988).
[32] C. Lee, W. Yang, and R. G. Parr, Phys. Rev. B **37**, 785 (1988).
[33] S. H.Vosko, L. Wilk, and M. Nusair, Can. J. Phys. **58**, 1200 (1980).
[34] C. H. Patterson, S. Banerjee, and J. F. McGilp, Phys. Rev. B **84**, 155314 (2011).
[35] *Physics of Group IV Elements and III-V Compounds, Landolt-Börnstein, New Series, Group III, Vol. 17, Part A*, edited by O. Madelung, M. Schulz, and H. Weiss (Springer-Verlag, New York, 1982).
[36] H. H. Weitering, X. Shi, and S. C. Erwin, Phys. Rev. B **54**, 10585 (1996).
[37] N. McAlinden and J. F. McGilp, Euro. Phys. Lett. **92**, 67008 (2010).